PHYSICAL REVIEW FLUIDS **2**, 122601(R) (2017)

Experimental quantification of nonlinear time scales in inertial wave rotating turbulence

Ehud Yarom, Alon Salhov, and Eran Sharon*
The Racah Institute of Physics, The Hebrew University of Jerusalem, Jerusalem 91904, Israel
(Received 18 December 2016; published 26 December 2017)

We study nonlinearities of inertial waves in rotating turbulence. At small Rossby numbers the kinetic energy in the system is contained in helical inertial waves with time dependence amplitudes. In this regime the amplitude variations time scales are slow compared to wave periods, and the spectrum is concentrated along the dispersion relation of the waves. A nonlinear time scale was extracted from the width of the spectrum, which reflects the intensity of nonlinear wave interactions. This nonlinear time scale is found to be proportional to $(\boldsymbol{U}\cdot\boldsymbol{k})^{-1}$, where $\boldsymbol{k}$ is the wave vector and $\boldsymbol{U}$ is the root-mean-square horizontal velocity, which is dominated by large scales. This correlation, which indicates the existence of turbulence in which inertial waves undergo weak nonlinear interactions, persists only for small Rossby numbers.

DOI: 10.1103/PhysRevFluids.2.122601

The study of rotating fluids is important to many fields such as engineering, geophysics, astrophysics, and more. Theoretical [1–4] and numerical studies [5–7] (see also [8], and references therein), as well as more recent experimental measurements [9], suggest that there is a regime in which rotating flows are turbulent while dominated by the propagation and interaction of inertial waves [10–13]. There is an active debate whether this is a valid description of such systems, or if their nature [14–17] (anisotropy with extreme amount of energy in two-dimensional (2D) modes, inverse energy cascade, and more) cannot be described in terms of interacting inertial waves [2,18,19]. In this Rapid Communication we experimentally determine the regime in which inertial waves that undergo weak nonlinear interactions dominate the three-dimensional (3D) part of the energy spectrum.

Incompressible fluids in rotating systems are described by the rotating Navier-Stokes equation (NSE) [8,20,21], resulting in two independent dimensionless parameters. In our experiment we use Reynolds number, $\mathrm{Re} = UL/\nu$ and Rossby number, $\mathrm{Ro} = U/(2\Omega L)$ (U and L are the typical velocity and length scales, ν is the kinematic viscosity, and $\Omega = |\boldsymbol{\Omega}|$ is the rotation rate of the system). In the conditions that characterize rotating turbulence $\mathrm{Re} \gg 1$ indicates dominance of nonlinear inertial effects over viscous effects, and $\mathrm{Ro} \ll 1$ indicates dominance of Coriolis acceleration over nonlinear inertial accelerations.

Under the above conditions the rotating NSE can be linearized, to have solutions in the form of plane inertial waves [20,21]. These waves, with frequency ω and wave vector $\boldsymbol{k}$, have a unique dispersion relation where ω does not depend on the wave number, $k = |\boldsymbol{k}|$, but only on its angle, θ, with the axis of rotation ($\boldsymbol{\Omega}$):

$$\omega = \pm 2\,\frac{\boldsymbol{\Omega}\cdot\boldsymbol{k}}{k} = \pm 2\Omega\,\cos(\theta). \tag{1}$$

The basic modes of these waves are helical modes [3,21–23]. These modes can be defined with helicity vectors:

$$\boldsymbol{h}_{\boldsymbol{k}}^{s} = \frac{1}{\sqrt{2}}\left(\frac{\boldsymbol{k}\times\boldsymbol{\Omega}}{|\boldsymbol{k}\times\boldsymbol{\Omega}|}\times\frac{\boldsymbol{k}}{|\boldsymbol{k}|} + is\,\frac{\boldsymbol{k}\times\boldsymbol{\Omega}}{|\boldsymbol{k}\times\boldsymbol{\Omega}|}\right), \tag{2}$$

*Corresponding author: erans@mail.huji.ac.il

 ©2017 American Physical Society

where $s = \pm 1$ is the helicity. The general velocity field can be represented by these modes using

$$\boldsymbol{u}(\boldsymbol{k},t) = a^{+}(\boldsymbol{k},t)\boldsymbol{h}^{+}(\boldsymbol{k}) + a^{-}(\boldsymbol{k},t)\boldsymbol{h}^{-}(\boldsymbol{k}), \tag{3}$$

where

$$a^{\pm} = \boldsymbol{u}\cdot\boldsymbol{h}^{\mp}. \tag{4}$$

For small but finite Rossby numbers inertial waves exist but the nonlinearity of the rotating NSE is not negligible. In such conditions the framework of wave turbulence might provide a valid description of the flow. Wave turbulence was predicted to appear in various physical systems [10–12] and was found experimentally in internal waves [24,25], surface waves [26–31], and elastic bending waves [32–35]. Recently, we showed experimentally that at Ro ~ 0.01 wave turbulence exists also in rotating turbulence [9]. It is not yet clear if inertial wave turbulence description can fully explain the unique properties of steady rotating turbulence. Simulation [5,6], theory [1–4,19,36], and experiments [9,18] (see also Ref. [8], and references within) in rotating systems suggest that wave turbulence does exist but provides only a limited description. Some works suggest wave turbulence cannot exist [18,19] or exists within a limited parameter regime [1,2,4,6]. In this Rapid Communication we identify two qualitatively different flow regimes. For small Ro the energy spectrum is concentrated around the dispersion relation of inertial waves. In this regime we identify the dominant nonlinear time scale, which is longer than the wave period. At large Ro, this time scale becomes short compared to the wave period, and the energy spectrum is no longer consistent with inertial waves dynamics.

The experimental setup is the one used in [9]. It is composed of a closed Plexiglass cylinder, 80 cm in diameter and 90 cm in height, which rotates up to 2 Hz along the $-\hat{z}$ axis. The tank contains water seeded with 50 μm polyamide particles which are used as tracers for flow visualization and measurement. Energy is injected homogenously at the bottom of the tank through a hexagonal layout of thin tubes. A closed circulation pump is injecting fluid in and out of the bottom through these tubes. The system works typically at Re $\sim 10^3$ and Ro $\sim 10^{-2}$–10^{-3}. All measurements presented here begin after waiting several minutes ($\geqslant$5 min) for the system to reach steady state (with constant rotation rate and energy injection rate). The experiment duration varies from $T = 45$ s to 150 s depending on Ω (covering at least 30 rotation periods).

A corotating camera above the cylinder captures frames at $\sim$750 frames/s. A vertical scanning horizontal laser sheet illuminates a specific height for each frame, sweeping over a total of 30 different heights ($55.5 < z < 81.3$ cm). The total measured volume is $V = 25.1 \times 25.1 \times 26.5$ cm^3. The velocity field is calculated using a standard 2D particle image velocimetry (PIV) technique, which provides the horizontal velocity components of the 3D measured volume (3D2C) (see Supplemental Material Movie M1 for an example of the energy density field dynamics [37]).

The main analysis is done by calculating the temporal-spatial Fourier transform of the velocity field: $u_i(\boldsymbol{k},\,\omega) = \mathcal{F}[\mathcal{W}(\boldsymbol{r})\cdot u_i(\boldsymbol{r},\,t)]$, where $\mathcal{W}(\boldsymbol{r})$ is a spatial windowing function (of type *Hamming*, normalized to conserve energy). The geometry of finite-size fluid volume is known to determine mode selection [1]. Still, Fourier transform analysis is used here since we study scaling laws of modes that are short compared to the system size.

We start by verifying that the wave field can be decomposed to two independent branches of positive and negative helicity. As in [9] we compute the energy spectrum in Fourier space as a functions of θ and ω:

$$E(\theta,\omega) = \frac{1}{2TV}\int_{k_{\min}}^{k_{\max}} dk \int_0^{2\pi} d\phi\, k^2 \sin(\theta)\left[u(\boldsymbol{k},\omega)_x^2 + u(\boldsymbol{k},\omega)_y^2\right]. \tag{5}$$

$k_{\min} = 1.33$ rad/cm is the minimal wave number with sufficient θ resolution, and $k_{\max} = 3.29$ rad/cm is the maximal measured wave number that exists in all directions. We find two distinct branches of energy [Fig. 1(a)] concentrated along the dispersion relation [Eq. (1)]. Incompressibility and Eq. (4) are used to decompose the data into positive and negative helical modes. The energy of

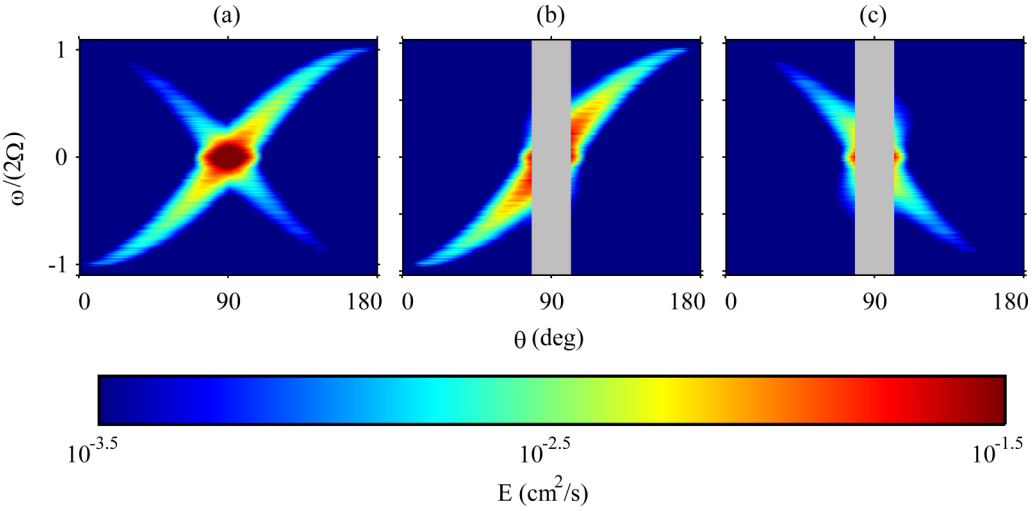

FIG. 1. (a) Horizontal velocity field energy spectrum $E(\theta,\omega)$ for $\Omega/2\pi = 1.5$ Hz and $\mathrm{Ro} = 8 \times 10^{-3}$. The energy in Fourier space is averaged on all ϕ and k (between $k_{\min} = 1.33$ and $k_{\max} = 3.29$ rad/cm), and plotted (logarithmic scale) as a function of $\omega/2\Omega$ and θ. (b) and (c) are the positive and negative helical modes $[E^s(\theta,\omega)]$. The gray area around $\theta \sim 90^\circ$ is not defined since $u_z(\theta \sim 90^\circ)$ cannot be calculated.

each mode is defined as $E^s(\theta,\omega) = \frac{1}{2TV}\int_{k_{\min}}^{k_{\max}} dk \int_0^{2\pi} d\phi\, k^2 \sin(\theta) a^s(\boldsymbol{k},\omega)^2$. As expected, we find that each branch of $E(\theta,\omega)$ relates to different helical mode [Figs. 1(b) and 1(c)]. As energy is injected at the bottom of the tank the waves propagating upward [Fig. 1(b)] are more intense than the downward propagating waves [Fig. 1(c)] (see Supplemental Material on helical modes group velocity [37]). Although these are the fundamental modes of the flow, their derivation produces relatively large numerical noise. Further analysis is therefore performed on the Fourier energy spectrum.

To see the spectrum k dependence we separate the integration over k in Eq. (5) to integration over small intervals, Δk, around k to produce $E_k(\theta,\omega)$ (see Supplemental Material on energy calculations for a detailed description [37]). Figure 2 shows $E_k(\theta,\omega)$ for a specific wave number in four different experiments (see also Supplemental Material Fig. S1 [37]). For the smallest Rossby number [Fig. 2(a)] the energy is highly concentrated along the inertial wave dispersion. As Ro increases [Figs. 2(b) and 2(c)] the spectrum broadens. For the largest Ro [Fig. 2(d)] the spectrum is widely spread and the dispersion relation is hardly visible.

The broadening of a spectrum indicates changes of wave amplitude and phase. In a system of interacting waves, amplitude modulations result from nonlinear wave interactions with typical time scale, τ_{NL}. For wave turbulence framework to be valid τ_{NL} must be long enough (i.e., small nonlinearity) compared to the wave period: $\tau_{\mathrm{NL}} \gg \tau_\omega$ (where $\tau_\omega = 2\pi/\omega$ is the wave period).

To identify τ_{NL} we examine the time dependence of a single Fourier mode. The velocity field is transformed in space, and we plot (the real part of) one wave vector, $\boldsymbol{k'} = (k',\theta',\phi')$, as a function of time, $\mathrm{Re}[u_x(\boldsymbol{k'},t)]$ [Fig. 3(a)]. Indeed, the mode oscillates in the wave frequency according to Eq. (1) (see inset), while large *amplitude* variations are clearly visible. In this example the typical modulation time scale (∼5 s) is significantly longer than the wave period. Figure 3(b) is the temporal spectrum of the signal in Fig. 3(a) [showing $u_x^2(\boldsymbol{k'},\omega)$]. For a linear system a delta function at $\omega = \omega_k$ is expected. The continuous changes in amplitude result in widening of the spectrum, where the width, $\Delta\omega$, is related to the time scale of the amplitude modulation, $\tau_{\mathrm{NL}} \sim \Delta\omega^{-1}$. It is important to note that the spectrum is broadened nearly symmetrically around $\omega_{\boldsymbol{k}}$, with no significant frequency shift (in contrast to other experiments [18]). This indicates that the deviation from the dispersion relation is indeed due to the relatively isotropic (in the horizontal plane) dynamics, and not due to strong mean flow, or other symmetry-breaking mechanisms.

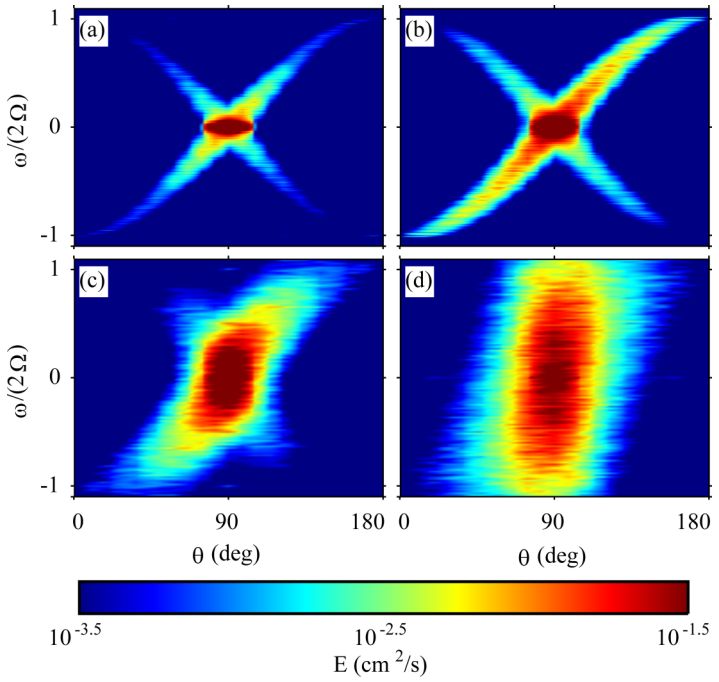

FIG. 2. Fourier energy spectra, $E_k(\theta,\omega)$ (logarithmic scale), for $k = 1.76$ rad/cm and different Ro (Ro = 0.004, 0.008, 0.02, 0.06). For small Ro, energy is concentrated around the inertial wave dispersion relation. As Ro increases, the energy spectrum spreads, until for very large Ro the dispersion relation is no longer a significant feature in the spectrum. See Supplemental Material Fig. S1 for more figures in a larger range of Ro and k [37].

The question of what processes determine and govern τ_{NL} is of major importance for the understanding of rotating turbulence. In such a complex system, many different nonlinear processes are possible, each with its typical scaling relation. A recent numerical study [6] found a regime in which $\tau_{\mathrm{NL}} \sim (Uk)^{-1}$, where U is the root-mean-square velocity and k is the wave number. This scaling was suggested to result from the drift, or sweeping, of the fast, short 3D inertial modes by the large-scale slow 2D part of the flow. Indirect evidence for frequency change due to sweeping effects was also found in experiments [18].

In order to identify the dominant nonlinearities in our experiments we study the variation of $\Delta\omega/\omega$ for each polar angle θ and wave number k, and for a total of 27 experiments with different Rossby and Reynolds numbers. The data from this broad range of parameters collapse onto a linear relation, which indicates $\tau_{\mathrm{NL}} \sim (U_\perp k_\perp)^{-1} \equiv \tau_U$, where $U_\perp = \sqrt{2\int\int\int dk\, d\theta\, d\omega\, E_k(\theta,\omega)}$ and $k_\perp$ is the horizontal component of the wave vector [note that in our system $(U_\perp k_\perp)^{-1} \approx (\boldsymbol{U}\cdot\boldsymbol{k})^{-1}$, since $\sim$90% of the energy is contained in nearly ($\pm 20^\circ$) horizontal modes; see Fig. 1(a)]. In this analysis both τ_{NL} and τ_U are calculated as the statistical means in a steady-state turbulence, using only the horizontal velocity fields.

The linear scaling holds for $(\tau_U\omega)^{-1} < 0.3$, for which the weak turbulence condition, $\Delta\omega < \omega$, is obeyed. The second regime corresponds to strong interactions with horizontal modes, such that $(\tau_U\omega)^{-1} > 0.3$. In this regime the nonlinear time scale is so small ($\tau_{\mathrm{NL}} < \tau_\omega$) that well-defined waves do not really exist.

In conclusion, we analyzed the spectral and time evolution of inertial waves within a rotating turbulence. We have shown experimentally the existence of a regime in which the 3D rotating turbulent field is well described as an ensemble of inertial waves that undergo weak nonlinear

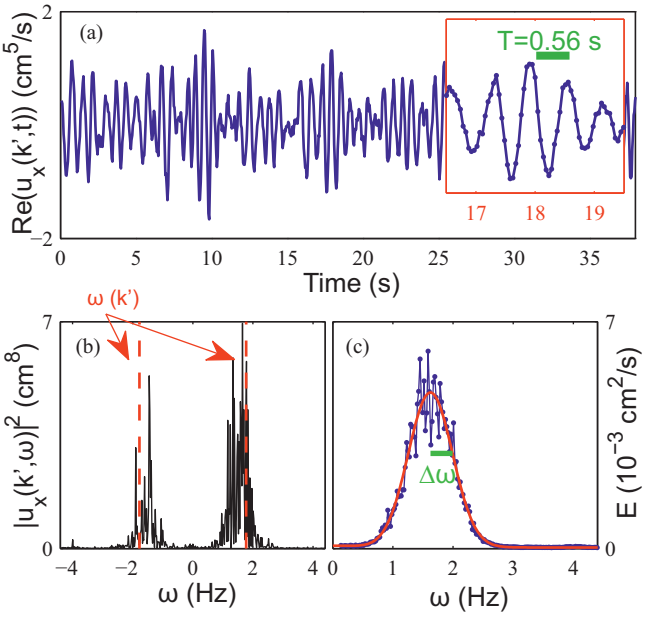

FIG. 3. Spatial Fourier of the velocity field for a single wave vector. (a) Real part of the Fourier transform of the velocity field in the x direction: $\mathrm{Re}[u_x(\boldsymbol{k}',t)]$, for $k' = 1.76$ rad/cm, $\theta' = 116^\circ, \phi' = 176^\circ$. Rotation frequency is $\Omega/2\pi = 2$ Hz. There is a main frequency governing the signal with amplitude modulations. The inset is a close-up, showing the governing oscillations with the expected period of 0.56 s [corresponding to $|\omega'| = 2\Omega\cos(\theta')$]. (b) Temporal Fourier spectrum of (a), showing $|u_x(\boldsymbol{k}',\omega)|^2$. There are two peaks specifying the positive and negative helical modes. Two vertical lines represent the expected frequency ω'. (c) Energy spectrum density integrated over ϕ for both u_x and u_y fields. Showing $E_{k'}(\theta',\omega)$ in blue for the positive mode only. The red line is the Gaussian fit with width $\Delta\omega$ (green line) defined as the standard deviation.

interactions. The dominant nonlinear processes in this regime are weak interactions of inertial waves with horizontal (or nearly horizontal) modes. The time scale that governs these interactions is $\tau_U = (U_\perp k_\perp)^{-1}$ and a robust linear relation between the broadening of the energy spectrum and τ_U^{-1} was found for $(\tau_U\omega)^{-1} < 0.3$. The nonlinear interactions in this regime are manifested by slow *amplitude* modulations of the 3D inertial modes, an effect which is not necessarily expected for slow sweeping of 3D modes by large-scale 2D modes. Still, the measured scaling can account for a variety of processes that are "mean-field-like". For $(\tau_U\omega)^{-1} > 0.3$, these nonlinear processes are fast compared to the wave period and the resemblance of the energy spectrum to the linear wave dispersion relation is lost. It is, therefore, clear that this weak turbulence of waves would not be detected in experiments (or simulations) that are limited in scale, or rotation rate: In order to be in the relevant regime, while having $\mathrm{Re} \sim 10^3$, there is a need for both rapid rotation (increasing ω) and a large system (small wave numbers, thus large τ_U). These are challenging requirements that are not easily met. Yet, the results of this work, together with the results of recent simulations [6] confirm the existence of a regime in which the inertial wave spectrum is dominated by weak nonlinear interactions, a regime which is most suitable for further theoretical study.

We are thankful to the anonymous referee who suggested that we test the scaling which leads to the data collapse in Fig. 4. This research was supported by the Israel Science Foundation, Grant No. 866/16.

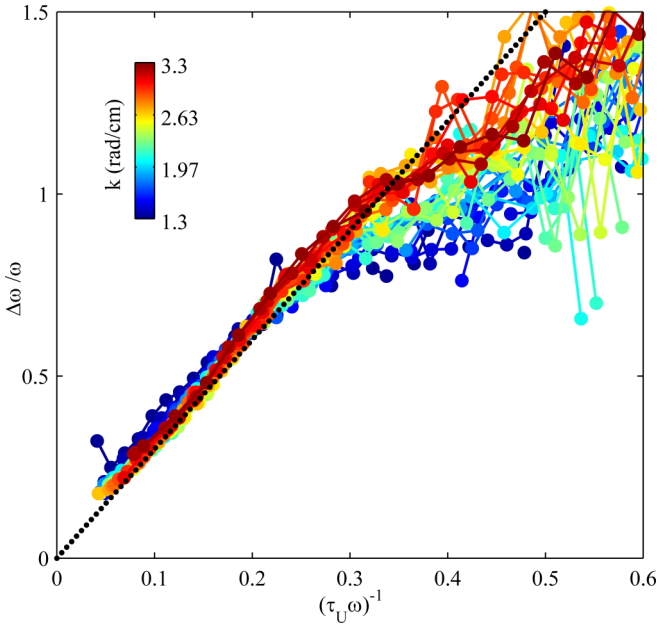

FIG. 4. Normalized spectra width as function of normalized interaction time scale for each k and θ [38], where $\tau_U^{-1} = Uk\sin\theta$. There is a strong correlation between the measured spectra width and τ_U^{-1}, indicating nonlinear interactions with mean flow are the main cause of spectrum broadening. The black dashed line represents $y = 3x$. The results show a good collapse of the data only for $\Delta\omega/\omega < 1$, where a perfect linear line is observed. For larger values the data is more spread. Thus we see two regimes, where weak nonlinearities with the horizontal modes exist only for $(\omega\tau_U)^{-1} < 0.3$.

[1] J. F. Scott, Wave turbulence in a rotating channel, J. Fluid Mech. **741**, 316 (2014).
[2] S. V. Nazarenko and A. A. Schekochihin, Critical balance in magnetohydrodynamic, rotating and stratified turbulence: Towards a universal scaling conjecture, J. Fluid Mech. **677**, 134 (2011).
[3] S. Galtier, Weak inertial-wave turbulence theory, Phys. Rev. E **68**, 015301(R) (2003).
[4] C. Cambon, R. Rubinstein, and F. S. Godeferd, Advances in wave turbulence: Rapidly rotating flows, New J. Phys. **6**, 73 (2004).
[5] F. Bellet, F. S. Godeferd, J. F. Scott, and C. Cambon, Wave turbulence in rapidly rotating flows, J. Fluid Mech. **562**, 83 (2006).
[6] P. Clark di Leoni, P. J. Cobelli, P. D. Mininni, P. Dmitruk, and W. H. Matthaeus, Quantification of the strength of inertial waves in a rotating turbulent flow, Phys. Fluids **26**, 35106 (2014).
[7] Y. Bin Baqui, P. A. Davidson, and A. Ranjan, Are there two regimes in strongly rotating turbulence?, Phys. Fluids **28**, 45103 (2016).
[8] F. S. Godeferd and F. Moisy, Structure and dynamics of rotating turbulence: A review of recent experimental and numerical results, Appl. Mech. Rev. **67**, 30802 (2015).
[9] E. Yarom and E. Sharon, Experimental observation of steady inertial wave turbulence in deep rotating flows, Nat. Phys. **10**, 510 (2014).
[10] V. E. Zakharov, V. S. L'vov, and G. Falkovich, *Kolmogorov Spectra of Turbulence I* (Springer, Berlin/ Heidelberg, 1992).
[11] A. C. Newell and B. Rumpf, Wave turbulence, Annu. Rev. Fluid Mech. **43**, 59 (2011).
[12] S. Nazarenko, *Wave Turbulence* (Springer, Berlin/ Heidelberg, 2011).
[13] S. Nazarenko, Wave turbulence, Contemp. Phys. **56**, 359 (2015).

[14] E. J. Hopfinger, F. K. Browand, and Y. Gagne, Turbulence and waves in a rotating tank, J. Fluid Mech. **125**, 505 (1982).
[15] E. Yarom, Y. Vardi, and E. Sharon, Experimental quantification of inverse energy cascade in deep rotating turbulence, Phys. Fluids **25**, 085105 (2013).
[16] A. Campagne, B. Gallet, F. Moisy, and P. Cortet, Direct and inverse energy cascades in a forced rotating turbulence experiment, Phys. Fluids **26**, 125112 (2014).
[17] L. Jacquin, O. Leuchter, C. Cambonxs, and J. Mathieu, Homogeneous turbulence in the presence of rotation, J. Fluid Mech. **220**, 1 (1990).
[18] A. Campagne, B. Gallet, F. Moisy, and P.-P. Cortet, Disentangling inertial waves from eddy turbulence in a forced rotating-turbulence experiment, Phys. Rev. E **91**, 043016 (2015).
[19] B. Gallet, Exact two-dimensionalization of rapidly rotating large-Reynolds-number flows, J. Fluid Mech. **783**, 412 (2015).
[20] H. P. Greenspan, *The Theory of Rotating Fluids*, Cambridge Monographs on Mechanics (Cambridge University Press, Cambridge, 1968).
[21] P. A. Davidson, *Turbulence in Rotating, Stratified and Electrically Conducting Fluids* (Cambridge University Press, Cambridge, 2013).
[22] F. Waleffe, Inertial transfers in the helical decomposition, Phys. Fluids A **5**, 677 (1993).
[23] F. Waleffe, The nature of triad interactions in homogeneous turbulence, Phys. Fluids **4**, 350 (1992).
[24] H. Scolan, E. Ermanyuk, and T. Dauxois, Nonlinear Fate of Internal Wave Attractors, Phys. Rev. Lett. **110**, 234501 (2013).
[25] T. Dauxois, C. Brouzet, E. Ermanyuk, S. Joubaud, D. Le Tourneau, and I. Sibgatullin, Energy cascade in internal wave attractors, Proc. IUTAM **20**, 120 (2017).
[26] R. Holt and E. Trinh, Faraday Wave Turbulence on a Spherical Liquid Shell, Phys. Rev. Lett. **77**, 1274 (1996).
[27] E. Falcon, Laboratory experiments on wave turbulence, Discr. Contin. Dyn. Syst. - Ser. B **13**, 819 (2010).
[28] M. Berhanu and E. Falcon, Space-time-resolved capillary wave turbulence, Phys. Rev. E **87**, 033003 (2013).
[29] C. Falcón, E. Falcon, U. Bortolozzo, and S. Fauve, Capillary wave turbulence on a spherical fluid surface in low gravity, Europhys. Lett. **86**, 14002 (2009).
[30] É. Falcon, C. Laroche, and S. Fauve, Observation of Gravity-Capillary Wave Turbulence, Phys. Rev. Lett. **98**, 094503 (2007).
[31] Q. Aubourg and N. Mordant, Nonlocal Resonances in Weak Turbulence of Gravity-Capillary Waves, Phys. Rev. Lett. **114**, 144501 (2015).
[32] A. Boudaoud, O. Cadot, B. Odille, and C. Touzé, Observation of Wave Turbulence in Vibrating Plates, Phys. Rev. Lett. **100**, 234504 (2008).
[33] N. Mordant, Are There Waves in Elastic Wave Turbulence?, Phys. Rev. Lett. **100**, 234505 (2008).
[34] P. Cobelli, P. Petitjeans, A. Maurel, V. Pagneux, and N. Mordant, Space-Time Resolved Wave Turbulence in a Vibrating Plate, Phys. Rev. Lett. **103**, 204301 (2009).
[35] N. Mordant, Fourier analysis of wave turbulence in a thin elastic plate, Eur. Phys. J. B **76**, 537 (2010).
[36] S. Galtier, Theory for helical turbulence under fast rotation, Phys. Rev. E **89**, 041001(R) (2014).
[37] See Supplemental Material at http://link.aps.org/supplemental/10.1103/PhysRevFluids.2.122601 for additional calculations and images: helical modes group velocity, energy k-dependence, and detailed view of the energy spectra for different parameters.
[38] The results shown are only those with good Gaussian fit with two conditions: (1) The Gaussian peak is not far from the expected wave frequency, large enough relative to constant in fit, and the width can be identified properly and distinguishable from the noise at $\omega = 0$. (2) The width value must obey $\Delta\omega/2\Omega > 0.14$, since lower values can be the result of spherical analysis and not necessarily physical spectrum width.